Electronic Supplementary Information

Crystalline-Amorphous Ni-Ni(OH)$_2$ Core-Shell Catalyst for Alkaline Hydrogen Evolution Reaction

Jing Hu,[a] Siwei Li,*[a] Yuzhi Li,[a] Jing Wang,[a] Yunchen Du,[a] Zhonghua Li,[b] Xijiang Han,[a] Jianmin Sun[a] and Ping Xu*[a]

Theoretical Simulation and Calculation.

The generalized gradient approximation (GGA) with the Perdew-Burke-Ernzerhof (PBE) exchange correlation function and a 320 eV cutoff for the plane-wave basis set were employed to calculate the adsorption energy by using Materials Studio software and Dmol3 module. While we have constructed the theoretical models to simulate the amorphous Ni(OH)$_2$ material, as well as amorphous NiO and crystalline Ni(OH)$_2$. In addition, the current distributions were simulated by COMSOL software and the one-dimensional linear electrical analysis (elan) model has been established. For simulating the electrode surface, a square two-dimensional domain of conductive material (Ni(OH)$_2$) has a DC voltage difference applied to it. Within the square domain, there are several nickel particles (circular inclusion). The interior of the inclusion has the different properties from the bulk.

The Calculation of Free Energies.

For all the studied systems, the free energies were evaluated by the formula:

$$\Delta G(H^*) = \Delta E(H^*) + \Delta ZPE - T\Delta S$$

where $\Delta E(H^*)$, ΔZPE and ΔS are the binding energy, zero point energy change and entropy change of H* adsorption, respectively. The binding energy can be calculated by the equation: [S1]

$$\Delta E(H^*) = E(surf+H^*) - E(surf) - 1/2\ E(H^*)$$

where E(surf) represents the energy of adsorption surface.

In this work, the TΔS and ΔZPE are obtained by following the scheme proposed by Nørskov *et al*.[S2] Specifically, ΔS can be got by the equation:

$$\Delta S = S(H^*) - 1/2\ S(H_2) \approx -1/2\ S(H_2)$$

In view of the negligible vibrational entropy of H*. Thus we can easily conclude that the corresponding TΔS is −0.205 eV, since $TS(H_2)$ is known to be 0.41 eV for H_2 at 300 K and 1 atm.[S2]

Additionally, through the equation:

$$\Delta ZPE = ZPE(H^*) - 1/2\ ZPE(H_2)$$

The calculated value was employed to estimate ΔZPE for H*. It is worth mentioning that our calculated $ZPE(H_2)$ value is about 0.2723 eV, which is equal to the one reported by Nørskov *et al*.[S2]

Table S3 presents all the computed ZPE(H*) for H* adsorbed on the surface of different models and the corresponding ΔZPE, as well as ΔE(H*) values. Therefore, we can obtain the free energy of H* (ΔG(H*)) to evaluate the HER activity of the amorphous $Ni(OH)_2$, amorphous NiO as well as crystalline $Ni(OH)_2$, which is usually considered as an effective descriptor for HER activity (a catalyst with ΔG(H*) ≈ 0 could be an excellent candidate for HER).[S2]

The Details of Simulating Current Distributions.

Stationary simulation.

First, two square regions containing semi-circle have been constructed:

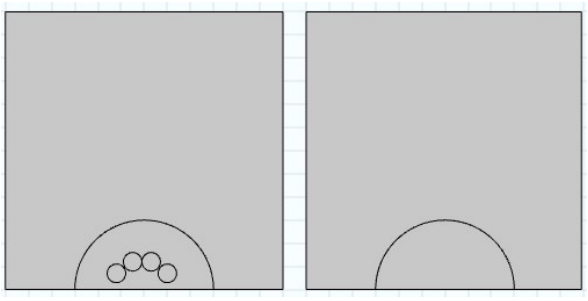

The squares represent the electrolytic cell; the semi-circles represent the amorphous $Ni(OH)_2$ shell; the four small circles represent the crystalline Ni particles. We use COMSOL 5.4 software, Electric Currents (ec) module and Stationary study. We used Finer Mesh to improve the simulation precision:

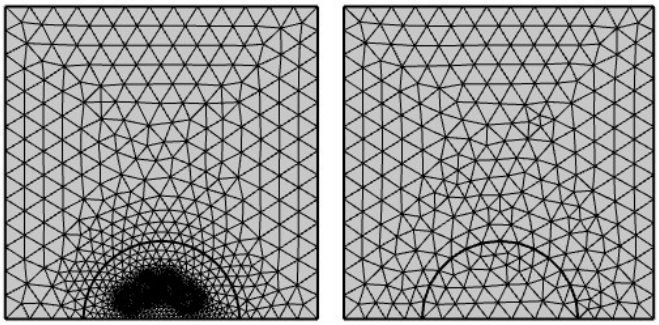

Time-dependent simulation.

The similar geometries have been used. We add two new modules to simulate the HER process: Tertiary Current Distribution, Nernst-Planck (tcd) and Electroanalysis (elan) modules. The following electrochemical reaction occurred at the $Ni(OH)_2$ surface:

$$2H^+ + 2e^- \rightarrow H_2$$

We use concentration dependent kinetics to simulate the reduction reaction, and the local current density has been set according to:

$$i_{loc,m} = i_{0,m}(C_{R,m}\exp\left(\frac{0.5F\eta_m}{RT}\right) - C_{O,m}\exp\left(-\frac{0.5F\eta_m}{RT}\right))$$

where $i_{0,m}$ is the exchange current density, $C_{R,m}$ is the reduced species expression, $C_{O,m}$ is the oxidized species expression and η_m is the overpotential for species m.

The over potential η_m is calculated from:

$$\eta_m = \phi_{s,ext} - \phi_l - E_{eq,m}$$

The equilibrium potential for the hydrogen reduction reaction is calculated using the Nernst Equation:

$$E_{eq,H} = E^{0}_{eq,H} + \frac{RT}{nF} ln[H^+]^2$$

The calculated value of $E_{eq,H}$ is about −1.42 V.

The time is in the range of 0−3000 s. The time step is 2.0 s.

Parameters.

Conductivity of Ni particles: 14.3×10^6 S/m;[S3]

Conductivity of $Ni(OH)_2$: 1×10^{-2} S/m;[S4]

The calculation details of Electrochemical active surface area (ECSA).

The cyclic voltammetry (CV) was used at non-Faradaic overpotentials as the means for estimating the effective electrochemical surface areas. The potential range of 0.045-0.145 V vs. RHE that tested at different scan rates (10, 20, 40, 60, 80 and 100 mV s^{-1}) were chosen. The differences in current density variation ($\Delta j = j_a - j_c$) at the potential of 0.1 V vs. RHE plotted against scan rate were fitted to estimate the electrochemical double-layer capacitance (C_{dl}), which was proportional to the electrochemical active surface area (ECSA) of the material. As the specific capacitance for a flat surface was generally found to be within the range of 20~60 μF cm^{-2}, therefore 40 μF cm^{-2} was used in the following calculations of the ECSA.

The ECSA is thus calculated from the following formula:

$$\mathrm{ECSA} = \frac{C_{\mathrm{dl}}}{40\mu\mathrm{F}\cdot\mathrm{cm}^{-2}\ \mathrm{per}\ \mathrm{cm}^2}$$

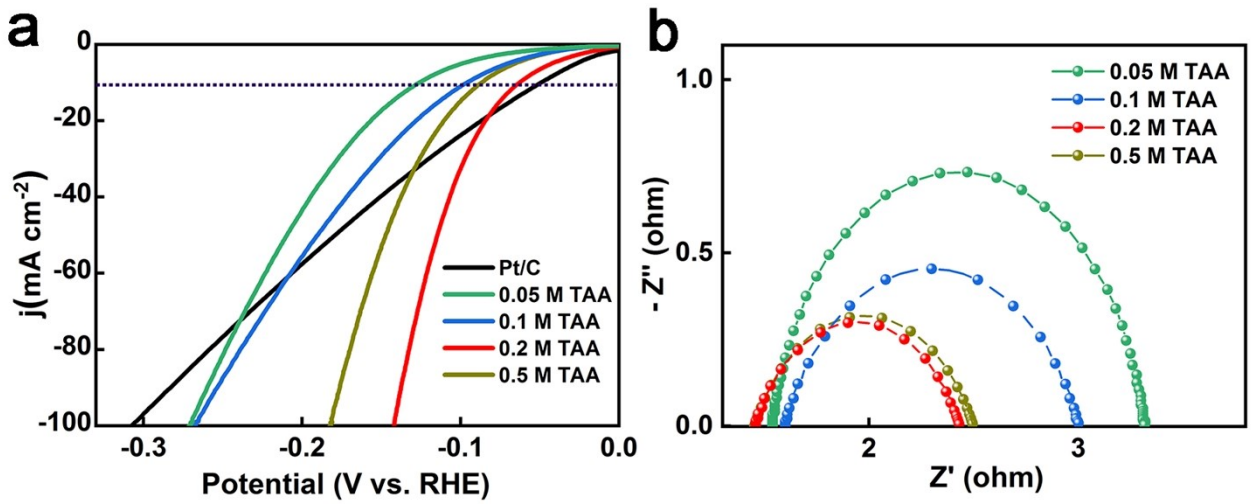

Fig. S1 Electrocatalytic performance of various samples when adding different amount of TAA for HER in 1.0 M KOH. (a) Linear sweep voltammetry (LSV) curves after *iR* correction, (b) electrochemical impedance spectroscopy.

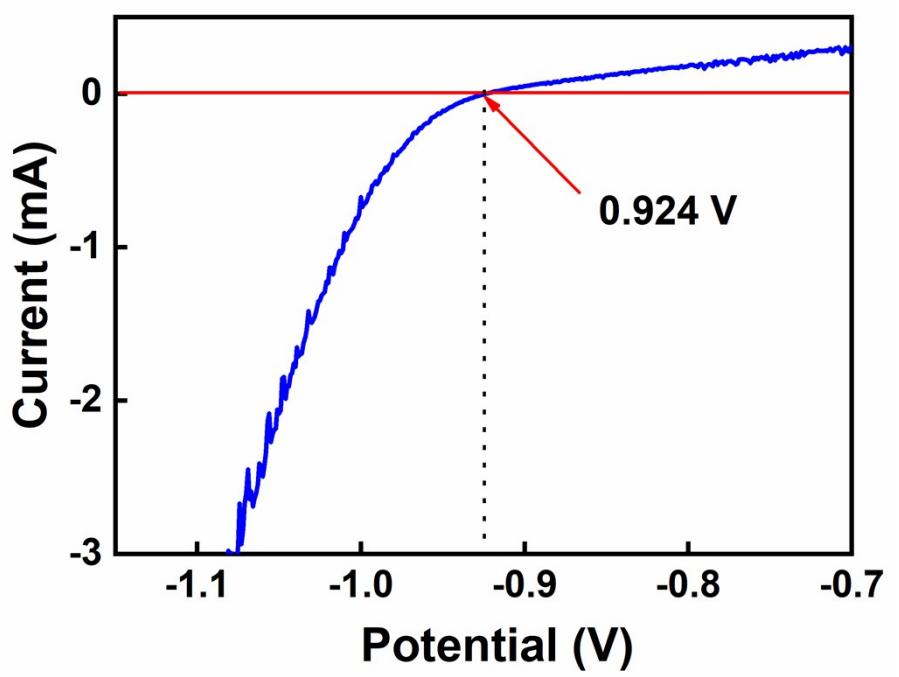

Fig. S2 Electrode calibration LSV curve of Hg/HgO in 1.0 M KOH (with a scan rate of 1 mV s^{-1} at room temperature of 20 ^{o}C).

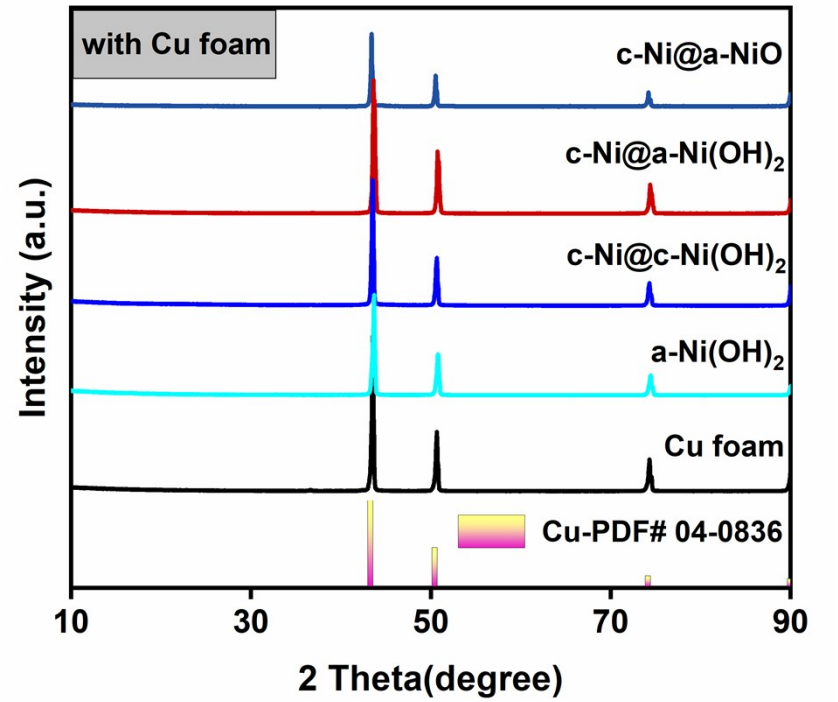

Fig. S3 XRD patterns of the prepared samples on Cu foam.

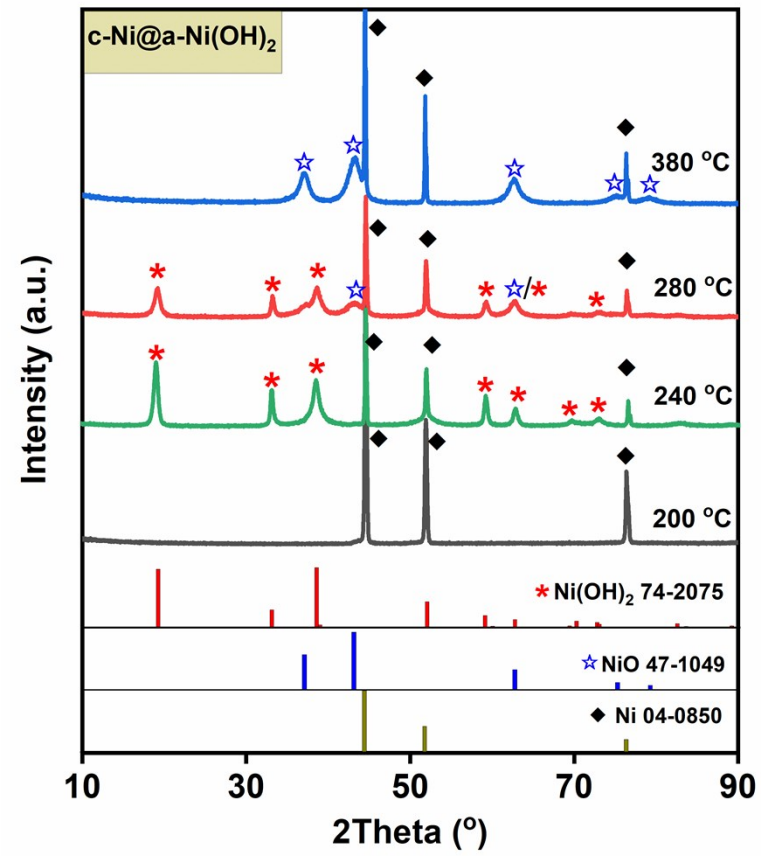

Fig. S4 XRD patterns of the c-Ni@a-$Ni(OH)_2$ under different heating temperatures.

When raising the temperature to 200 °C, only the diffraction peaks indexed to Ni were observed. When the temperature was further raised to 240 °C, peaks indexed to $Ni(OH)_2$ can be observed besides peaks indexed to Ni. When the crystallization process was performed at 280 °C, a small amount of NiO were observed besides metallic Ni and $Ni(OH)_2$. Further raising the temperature to 380 °C, the peaks indexed to $Ni(OH)_2$ disappears and the sample consists only crystalline Ni and NiO. Based on this experiment, we carried out the crystallization experiment of c-Ni@a-$Ni(OH)_2$ at 240 °C to obtain c-Ni@c-$Ni(OH)_2$.

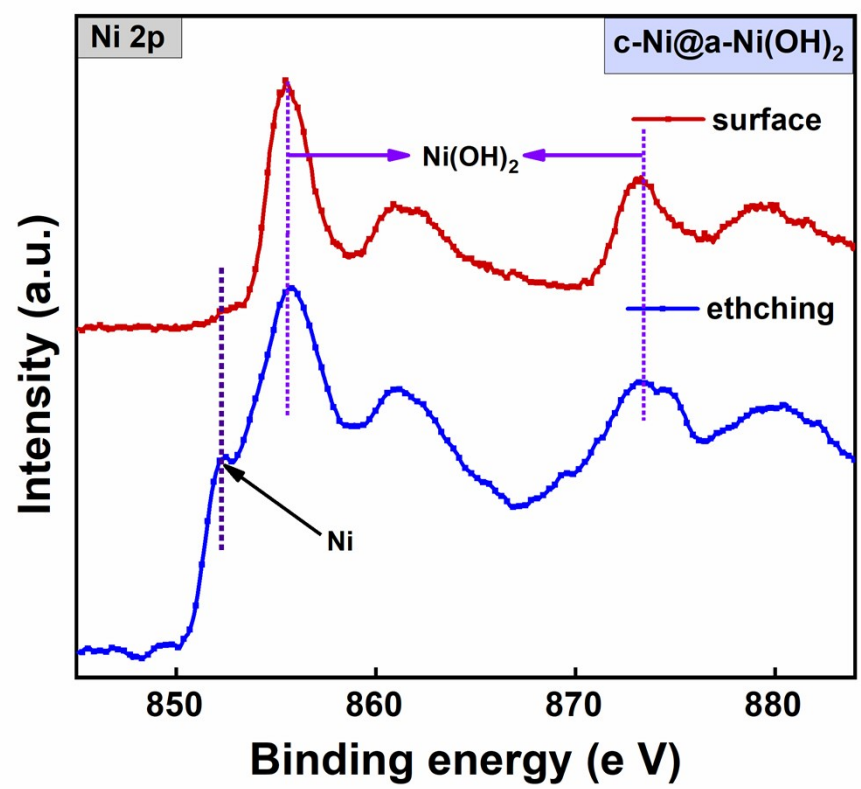

Fig. S5 XPS survey spectra of Ni 2p of the surface and etched surface after 30 seconds in sample of c-Ni@a-$Ni(OH)_2$.

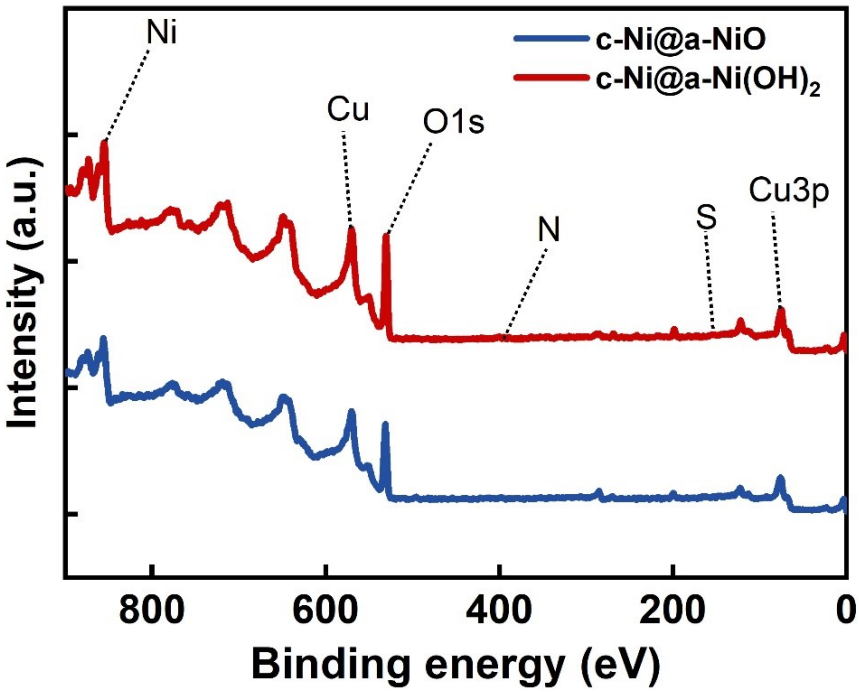

Fig. S6 XPS survey scans of c-Ni@a-NiO and c-Ni@a-$Ni(OH)_2$.

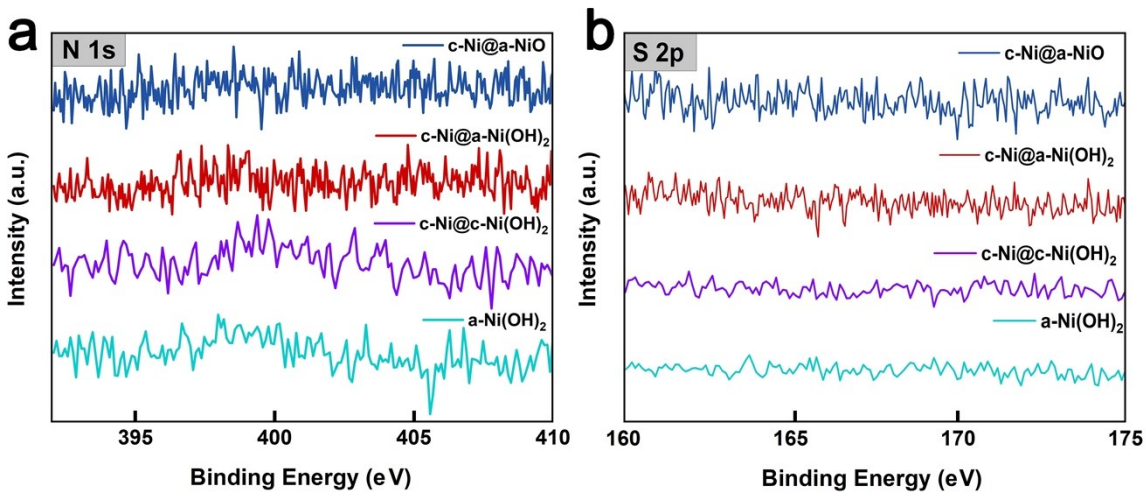

Fig. S7 XPS spectra of N 1s and S 2p of c-Ni@a-NiO, c-Ni@a-$Ni(OH)_2$, c-Ni@c-$Ni(OH)_2$, and a-$Ni(OH)_2$.

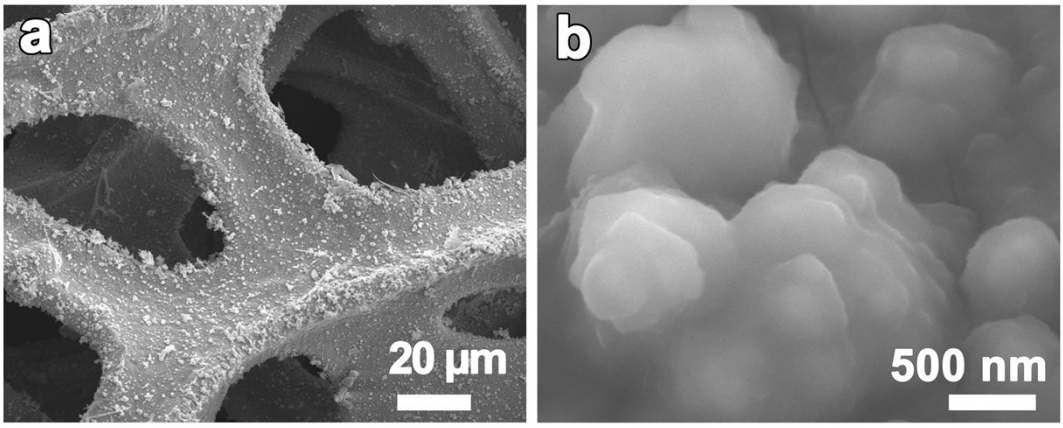

Fig. S8 SEM images of samples of c-Ni@a-NiO (a and b).

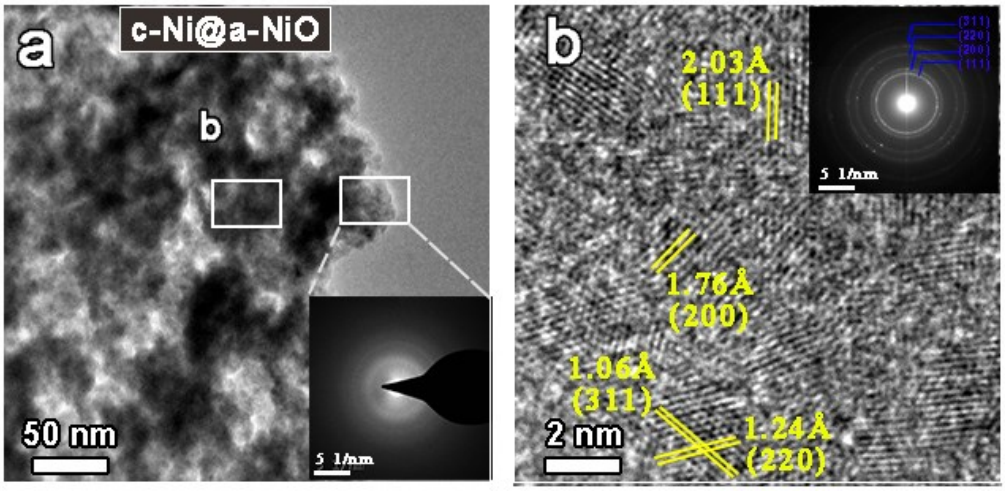

Fig. S9 TEM and HRTEM images of c-Ni@a-NiO (a and b). Without using TAA, the metallic Ni with large particle size in the sample had insufficient contact with around amorphous materials, leading to the oxidation of metallic Ni in the air.

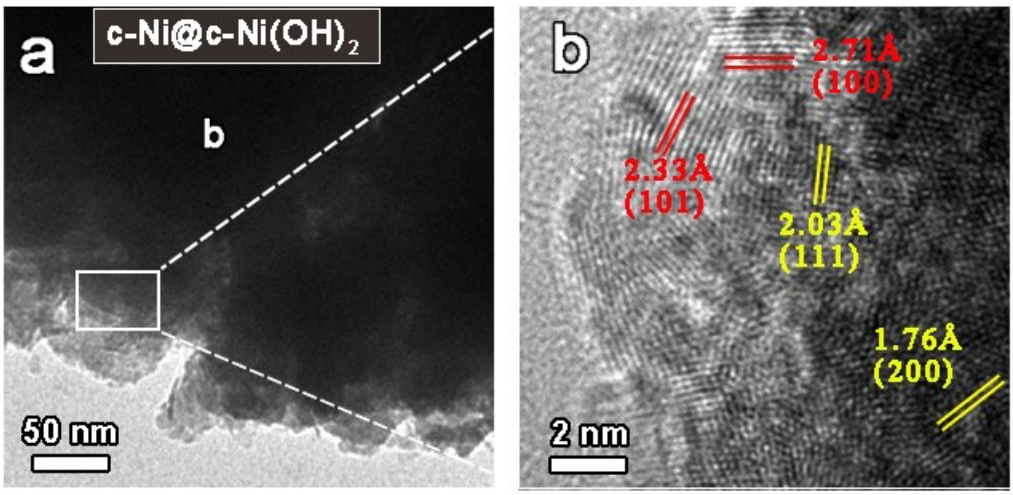

Fig. S10 TEM and HRTEM images of c-Ni@c-Ni(OH)$_2$.

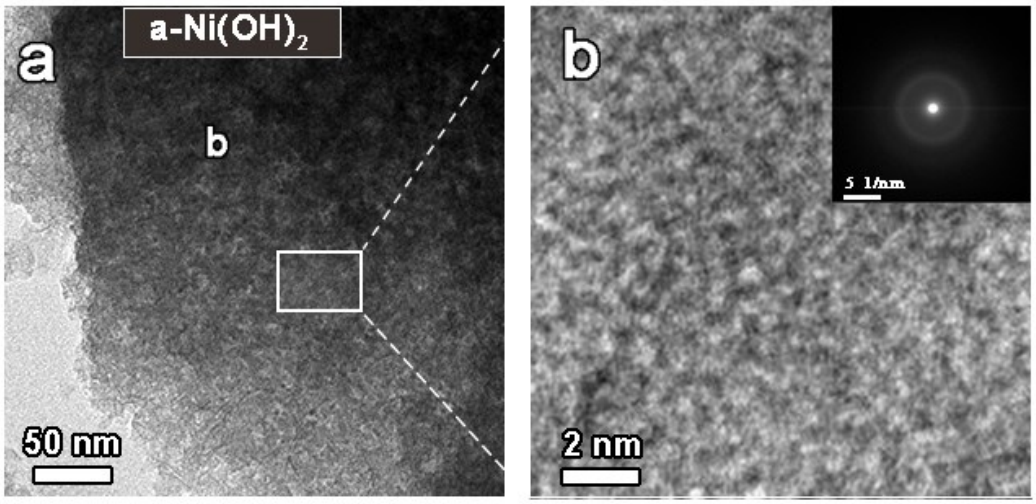

Fig. S11 TEM and HRTEM images of a-Ni(OH)$_2$.

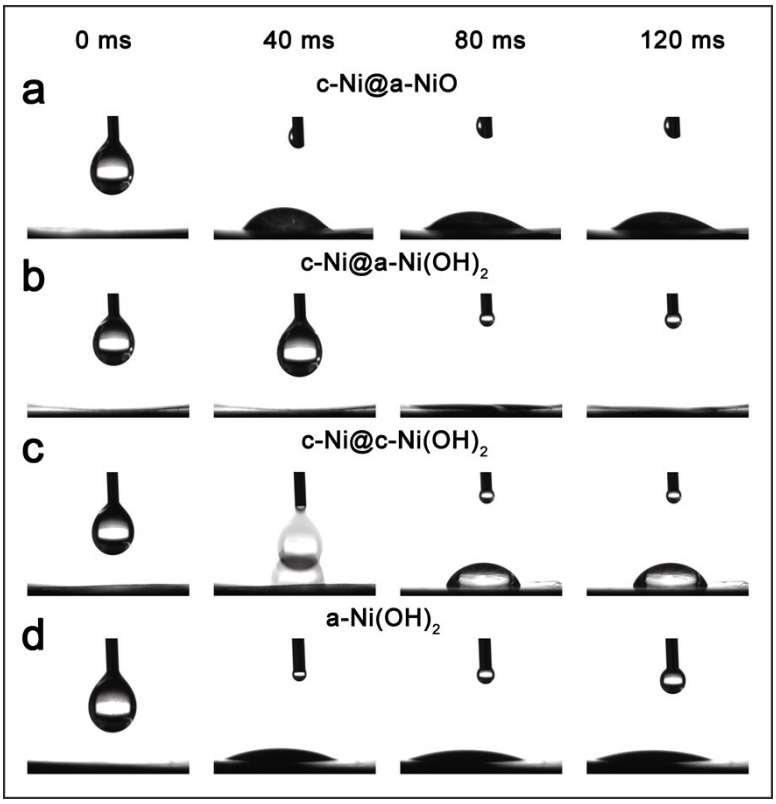

Fig. S12 Contact angle measurement of samples c-Ni@a-NiO (a), c-Ni@a-$Ni(OH)_2$ (b), c-Ni@c-$Ni(OH)_2$ (c), and a-$Ni(OH)_2$ (d) (using a drop of 1.0 M KOH solution).

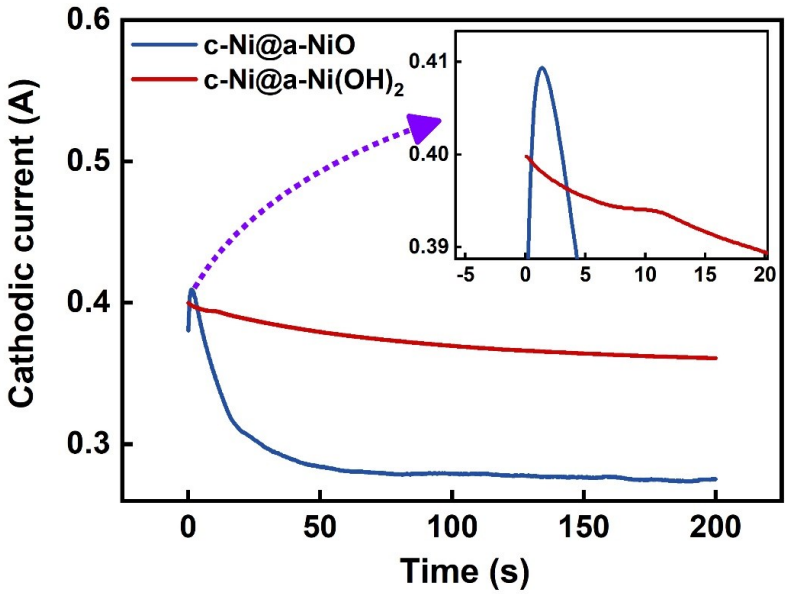

Fig. S13 Electrodeposition *i-t* curves of Cu foam electrode in solution of $NiCl_2$ (for preparing c-Ni@a-NiO) and $NiCl_2$/TAA (for preparing c-Ni@a-$Ni(OH)_2$).

The electrodeposition *i-t* curves in aqueous solution of $NiCl_2$ and $NiCl_2$/TAA were obtained under a potential of -1.2 V. As for the obtained curves in aqueous solution of $NiCl_2$, in the initial stage of electrodeposition, a sharp current peak is observed, giving the fact that the electrodeposition speed is very fast at the beginning of the stage. When using aqueous solution of $NiCl_2$/TAA, no obvious sharp current peak rather than a flat current platform appeared during the initial stage of electrodeposition (Inset of Fig. S13), indicating a slower electrodeposition speed.

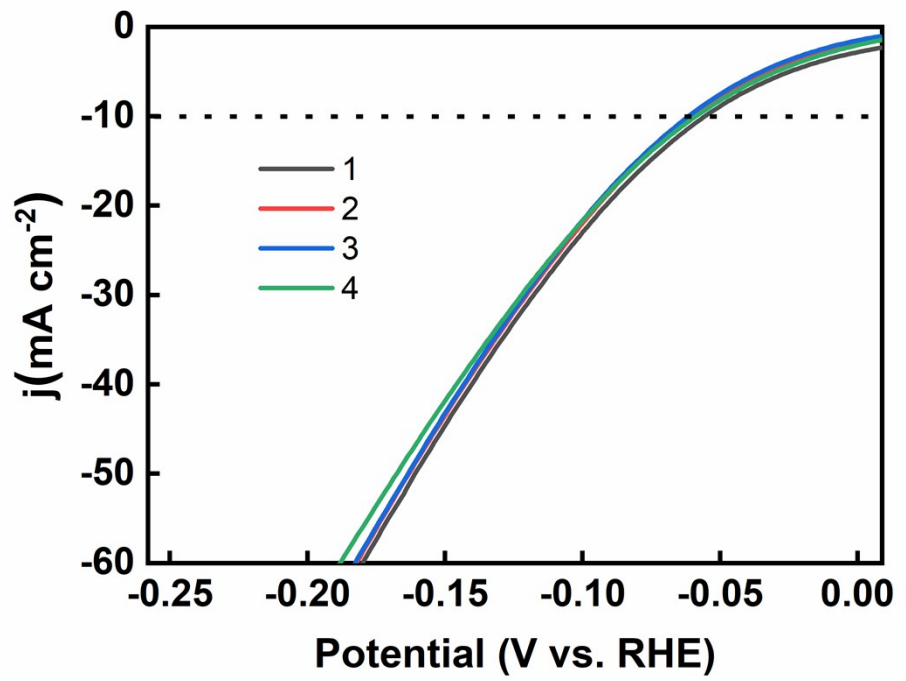

Fig. S14 LSV curves of the c-Ni@a-$Ni(OH)_2$ measured from samples from four different batches for HER in 1.0 M KOH.

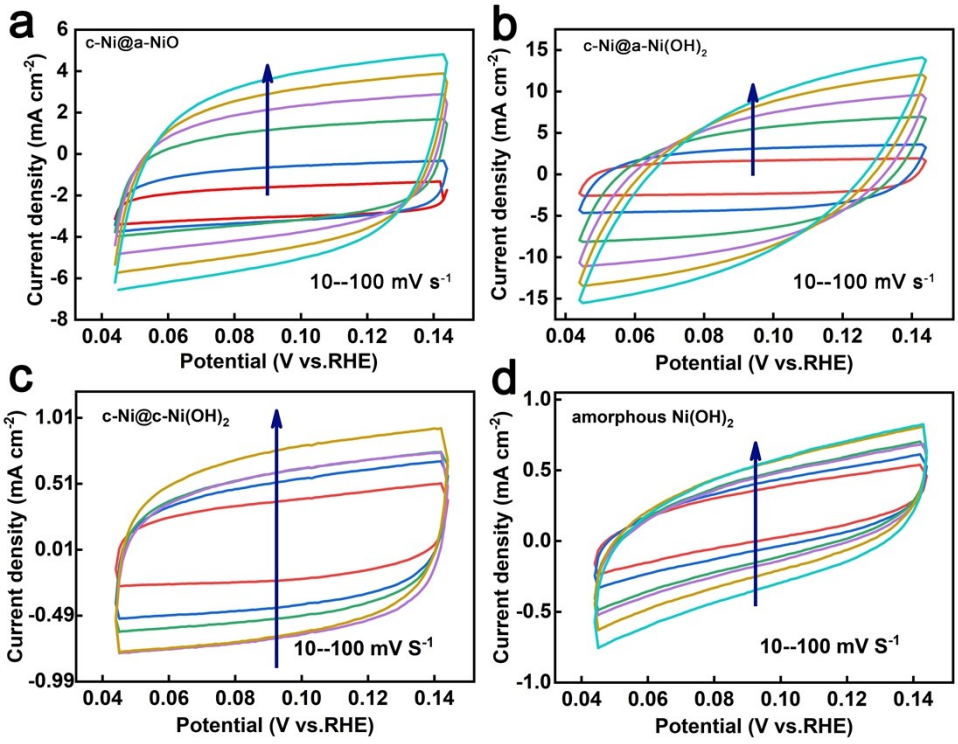

Fig. S15 CV curves of c-Ni@a-NiO (a), c-Ni@a-$Ni(OH)_2$ (b), c-Ni@c-$Ni(OH)_2$ (c), and a-$Ni(OH)_2$ (d) at various scan rates (10, 20, 40, 60, 80, and 100 mV s^{-1}) in the potential range of 0.045−0.145 V vs. RHE, which were used to estimate the double-layer capacitance (C_{dl}).

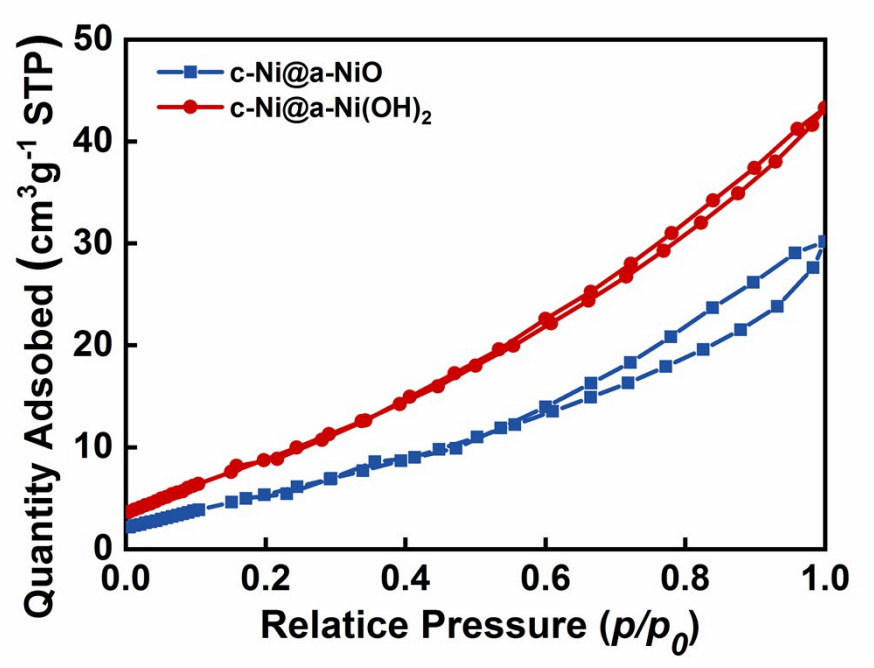

Fig. S16 N_2 adsorption-desorption isotherm of samples of c-Ni@a-NiO and c-Ni@a-$Ni(OH)_2$.

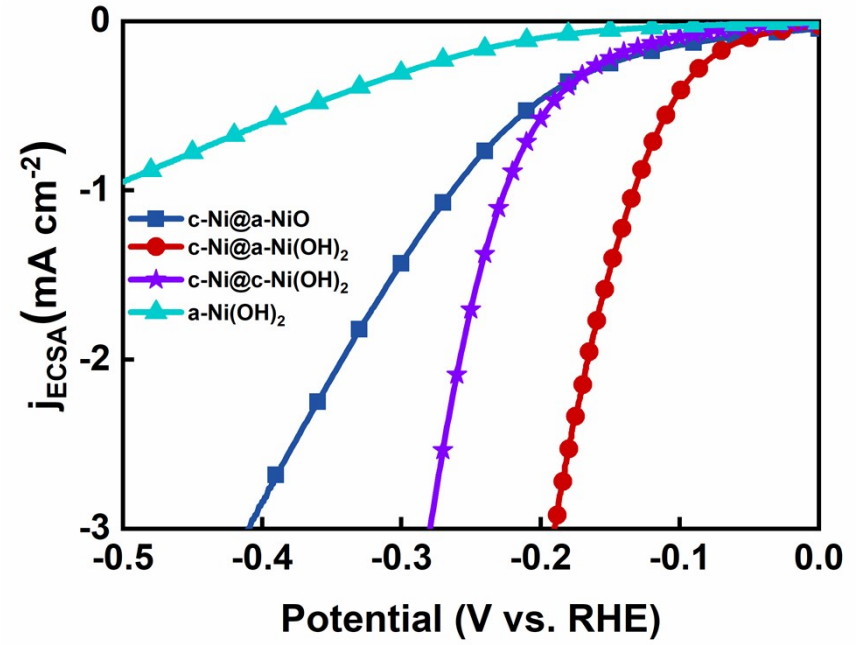

Fig. S17 The ECSA-normalized HER polarization curves of the prepared samples.

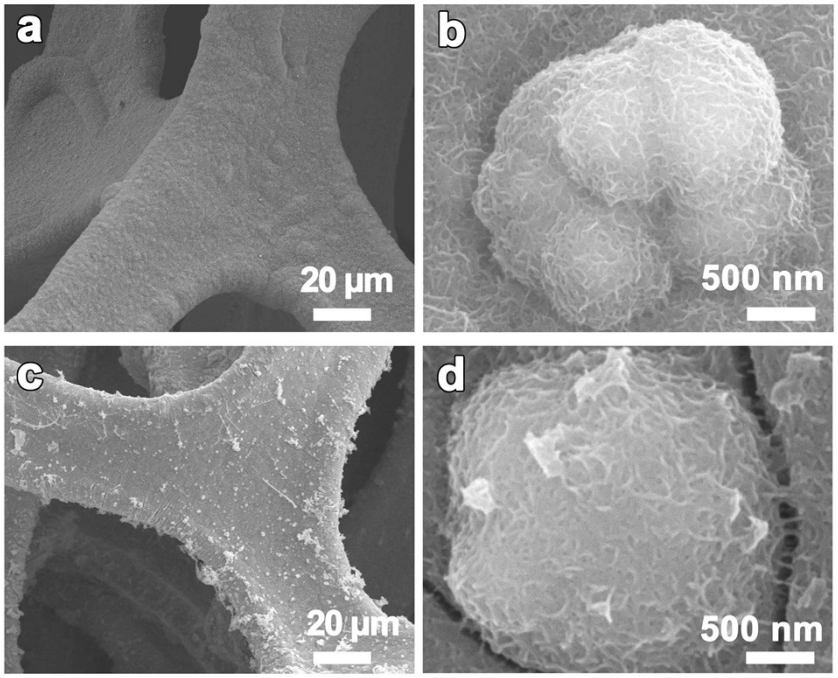

Fig. S18 SEM images of c-Ni@a-Ni(OH)$_2$/CF before and after being used in 1000 cycles of HER in 1.0 M KOH solution.

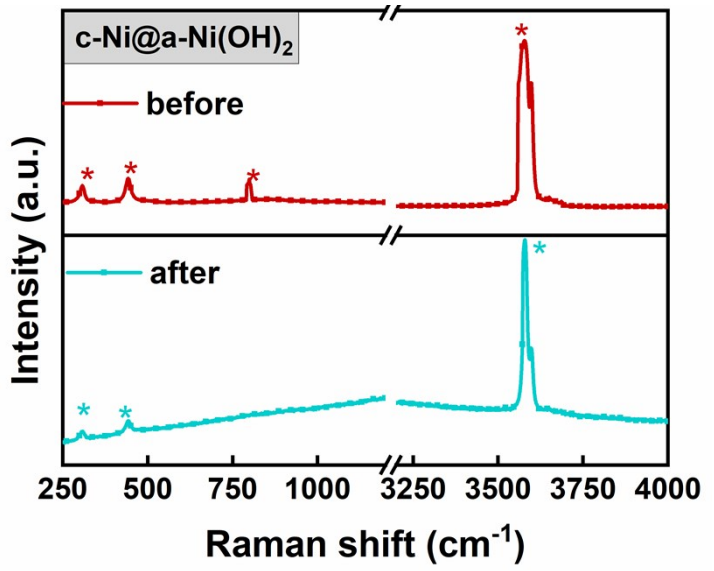

Fig. S19 Raman spectra of the material before and after catalysis.

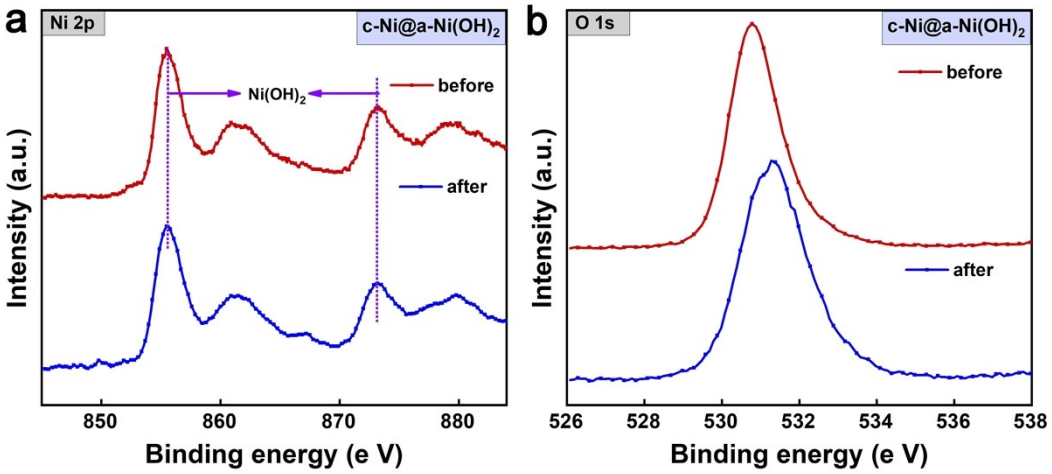

Fig. S20 X-ray photoelectron spectra of c-Ni@a-Ni(OH)$_2$/CF before and after 1000 cycles of electrocatalytic HER in 1.0 M KOH solution.

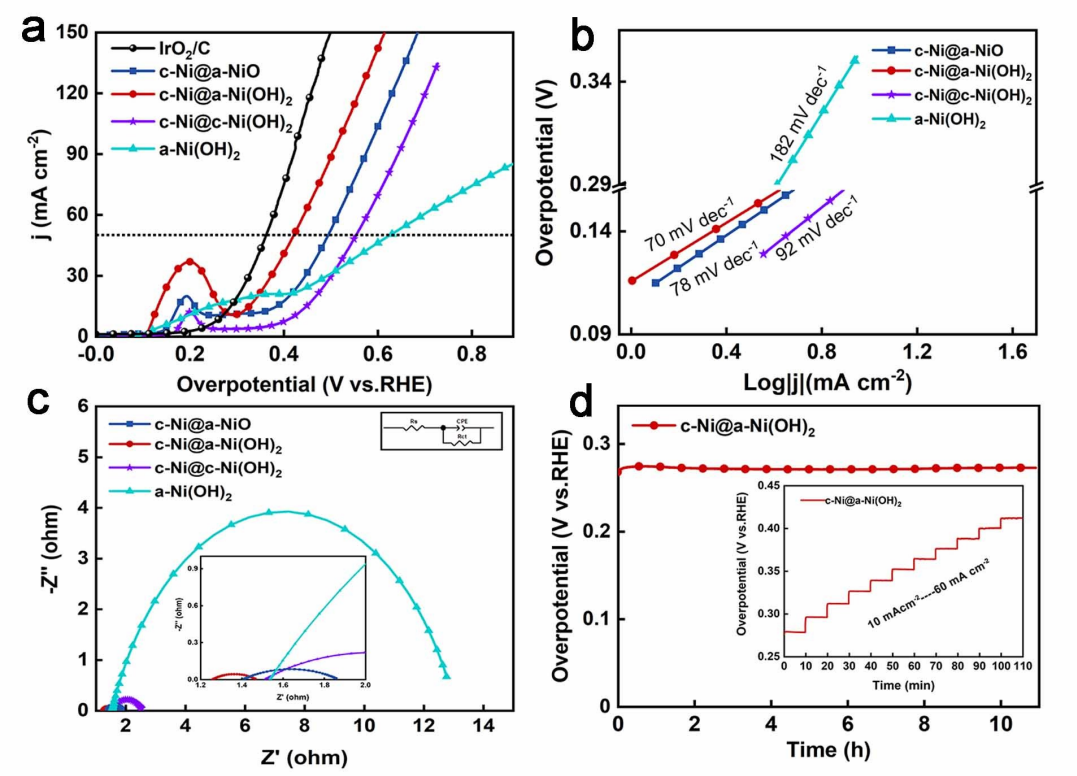

Fig. S21 Electrochemical properties of of c-Ni@a-NiO, c-Ni@a-Ni(OH)$_2$, c-Ni@c-Ni(OH)$_2$, and a-Ni(OH)$_2$ for OER catalysis in 1.0 M KOH. (a) Polarization curves after *iR* correction, in comparison to IrO_2/C; (b) Tafel plots; (c) electrochemical impedance spectroscopy Nyquist plots; and (d) Long-term durability tests of c-Ni@a-Ni(OH)$_2$ at a current density of 10 mA cm^{-2} for >10 h. (Inset shows the muti-step chronoamperometric curves of the c-Ni@a-Ni(OH)$_2$/CF in 1.0 M KOH. The current density started at 10 mA cm^{-2} and finished at 60 mA cm^{-2}, with an increment of 5 mA cm^{-2} after every 600 s.)

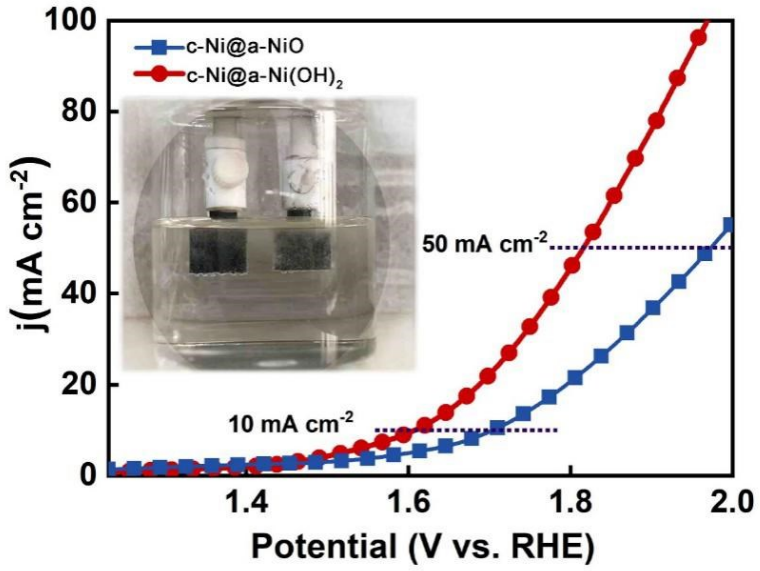

Fig. S22 Overall Water Splitting activities of the prepared samples.

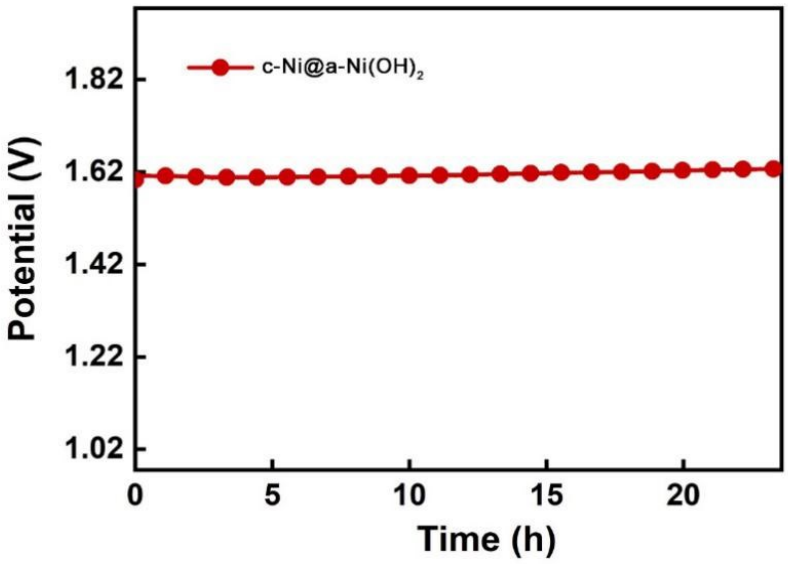

Fig. S23 Long-term stability of the c-Ni@a-$Ni(OH)_2$ electrode in an alkaline electrolyzer under a constant current density of 10 mA cm^{-2}, measured over 24 h.

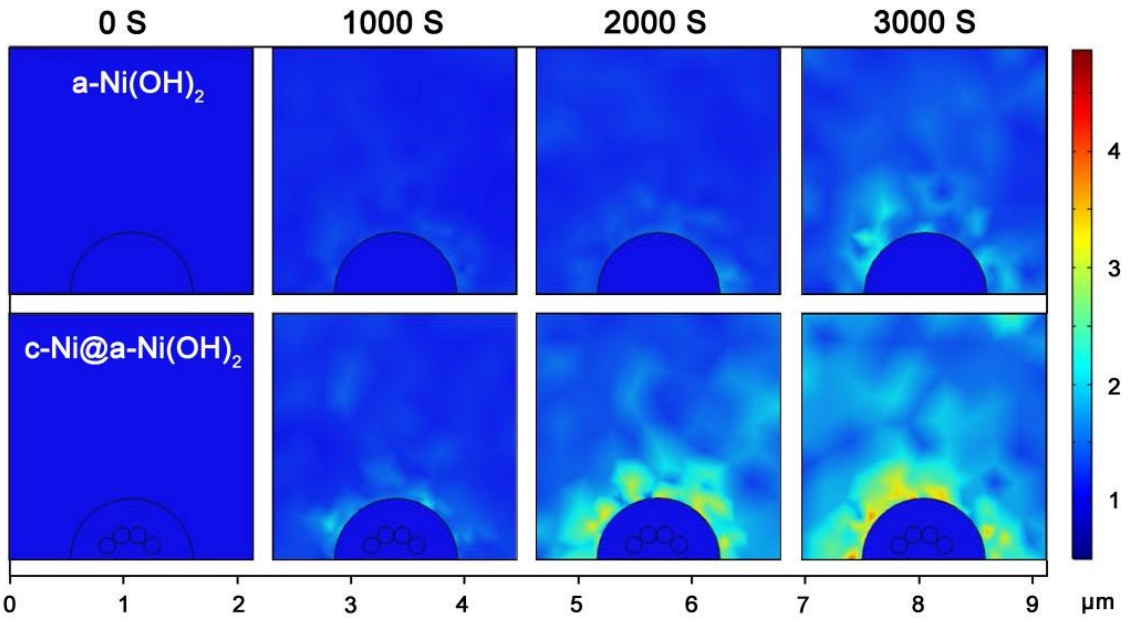

Fig. S24 The electrolyte current density plot during hydrogen evolution.

Table S1 Comparison of our overpotential of HER with other references.

Numbers	Overpotential	Materials	Mass loading	References
1	57 mV at 10 mA cm^{-2} 82 mV at 20 mA cm^{-2} 142 mV at 100 mA cm^{-2}	c-Ni@a-$Ni(OH)_2$	5.03 mg cm^{-2}	This work
2	66 mV at 10 mA cm^{-2}	Ni_2P-$NiSe_2$	9.2 mg cm^{-2}	[S5]
3	270 mV at 20 mA cm^{-2}	$Ni(OH)_2/Ni_3S_2$	/	[S6]
4	78 mV at 10 mA cm^{-2}	Ni_3S_2/MoS_2	8.6 mg cm^{-2}	[S7]
5	172 mV at 20 mA cm^{-2}	hydrotalcite-like $Ni(OH)_2$	2.9 mg cm^{-2}	[S8]
6	82 mV at 10 mA cm^{-2}	Ni@NC@MoS_2	0.28 mg cm^{-2}	[S9]
7	72 mV at 20 mA cm^{-2}	$Ni(OH)_2$–Ni_3N nanoarray	3.2 mg cm^{-2}	[S10]
8	105 mV at 10 mA cm^{-2}	3D-NiCoP	/	[S11]
9	80 mV at 10 mA cm^{-2}	2D Ni-thiolate nanosheets	0.53 mg cm^{-2}	[S12]

10	147 mV at 10 mA cm^{-2}	Ni–N_x species anchored porous carbon	/	[S13]
11	95 mV at 10 mA cm^{-2}	Ni-doped FeP/C hollow nanorods	0.4 mg cm^{-2}	[S14]
12	78 mV at 10 mA cm^{-2}	Ni foam supported Ni_2P nanosheets with Cu atoms	/	[S15]
13	87 mV at 10 mA cm^{-2}	Ni_5P_4@$Ni_{2+\delta}O_\delta(OH)_{2-\delta}$ with 3 nm amorphous layer	/	[S16]
14	93.4 mV at 10 mA cm^{-2}	Ni-Co-MoS_x ball-in-ball hollow nanospheres	0.365 mg cm^{-2}	[S17]
15	94 mV at 10 mA cm^{-2}	WS_2 on mesoporous 3D Ni_5P_4-Ni_2P structures	6.02 mg cm^{-2}	[S18]
16	77 mV at 10 mA cm^{-2}	Ultrathin Ni(0)-Embedded $Ni(OH)_2$ Heterostructured Nanosheets	0.5 mg cm^{-2}	[S19]
17	110 mV at 5 mA cm^{-2}	Crystalline/amorphous Ni/NiO core/shell nanosheets	0.3 mg cm^{-2}	[S20]
18	~100 mV at 10 mA cm^{-2}	Ni/NiO/CNT	8 mg cm^{-2}	[S21]
19	90 mV at 10 mA cm^{-2}	Ni/NiO-3.8	0.8 mg cm^{-2}	[S22]

Table S2 BET specific surface area and porosity of samples.

samples	[a]S_{BET} (m^2 g^{-1})	[b]V_t (cm^3 g^{-1})
c-Ni@a-NiO	23.839	0.0060
c-Ni@a-$Ni(OH)_2$	39.079	0.0117

[a] BET specific surface area (S_{BET}).

[b] Total pore volume (V_t).

Table S3 Impedance parameter values derived from the fitting to the equivalent circuit for the impedance spectra recorded in 1.0 M KOH solution.

samples	R_s	R_{ct}
c-Ni@a-NiO	1.542 Ω	2.56 Ω
c-Ni@a-$Ni(OH)_2$	1.533 Ω	0.98 Ω

c-Ni@c-Ni(OH)$_2$	1.561 Ω	0.70 Ω
a-Ni(OH)$_2$	1.554 Ω	21.5 Ω

Table S4 The calculated parameters of adsorbed H* at different active sites.

Models	ΔE(H*) (eV)	ZPE(H*) (eV)	ΔZPE (eV)	ΔG(H*) (eV)
Crystalline Ni(OH)$_2$	0.56	0.26	0.13	0.89
Amorphous NiO	0.33	0.17	0.14	0.67
Amorphous Ni(OH)$_2$	–0.16	0.17	0.04	0.16

References

S1 A. Jalil, Z. Zhuo, Z. Sun, F. Wu, C. Wang and X. Wu, *J. Mater. Chem. A*, 2020, **8**, 1307-1314.

S2 J. K. Nørskov, T. Bligaard, A. Logadottir, J. Kitchin, J. G. Chen, S. Pandelov and U. Stimming, *J. Electrochem. Soc.*, 2005, **152**, J23-J26.

S3 D. Li, D. Sutton, A. Burgess, D. Graham and P. D. Calvert, *J. Mater. Chem.*, 2009, **19**, 3719-3724.

S4 H. Guan, H. Wang, Y. Zhang, C. Dong, G. Chen, Y. Wang and J. Xie, *Appl. Surf. Sci.*, 2018, **447**, 261-268.

S5 C. Liu, T. Gong, J. Zhang, X. Zheng, J. Mao, H. Liu, Y. Li and Q. Hao, *Appl. Catal. B: Environ.*, 2020, **262**, 118245.

S6 X. Du, Z. Yang, Y. Li, Y. Gong and M. Zhao, *J. Mater. Chem. A*, 2018, **6**, 6938-6946.

S7 C. Wang, X. Shao, J. Pan, J. Hu and X. Xu, *Appl. Catal. B: Environ.*, 2020, **268**, 118435.

S8 Y. Rao, Y. Wang, H. Ning, P. Li and M. Wu, *ACS Appl. Mater. Interfaces*, 2016, **8**, 33601-33607.

S9 S. A. Shah, X. Shen, M. Xie, G. Zhu, Z. Ji, H. Zhou, K. Xu, X. Yue, A. Yuan and J. Zhu, *Small*, 2019, **15**, 1804545.

S10 M. Gao, L. Chen, Z. Zhang, X. Sun and S. Zhang, *J. Mater. Chem. A*, 2018, **6**, 833-836.

S11 B. Ma, Z. Yang, Y. Chen and Z. Yuan, *Nano Res.*, 2019, **12**, 375-380.

S12 C. Hu, Q. Ma, S.-F. Hung, Z.-N. Chen, D. Ou, B. Ren, H. M. Chen, G. Fu and N. Zheng, *Chem*, 2017, **3**, 122-133.

S13 C. Lei, Y. Wang, Y. Hou, P. Liu, J. Yang, T. Zhang, X. Zhuang, M. Chen, B. Yang and L. Lei, *Energy Environ. Sci.*, 2019, **12**, 149-156.

S14 X. F. Lu, L. Yu and X. W. D. Lou, *Sci. Adv.*, 2019, **5**, eaav6009.

S15 S. Chu, W. Chen, G. Chen, J. Huang, R. Zhang, C. Song, X. Wang, C. Li and K. K. Ostrikov, *Appl. Catal. B: Environ.*, 2019, **243**, 537-545.

S16 Y. Huang, L. Hu, R. Liu, Y. Hu, T. Xiong, W. Qiu, M.-S. J. T. Balogun, A. Pan and Y. Tong, *Appl. Catal. B: Environ.*, 2019, **251**, 181-194.

S17 X. Qian, C. Xu, Y. Jiang, J. Zhang, G. Guan and Y. Huang, *Chem. Eng. J.*, 2019, **368**, 202-211.

S18 S. H. Yu, W. Chen, H. Wang, H. Pan and D. H. Chua, *Nano Energy*, 2019, **55**, 193-202.

S19 L. Dai, Z. N. Chen, L. Li, P. Yin, Z. Liu and H. Zhang, *Adv. Mater.*, 2020, **32**, 1906915.

S20 X. Yan, L. Tian and X. Chen, *J. Power Sources*, 2015, **300**, 336-343.

S21 M. Gong, W. Zhou, M.-C. Tsai, J. Zhou, M. Guan, M.-C. Lin, B. Zhang, Y. Hu, D.-Y. Wang, J. Yang, S. J. Pennycook, B.-J. Hwang and H. Dai, *Nat. Commun.*, 2014, **5**, 4695.

S22 L. Zhao, Y. Zhang, Z. Zhao, Q.-H. Zhang, L.-B. Huang, L. Gu, G. Lu, J.-S. Hu and L.-J. Wan, *Natl. Sci. Rev.*, 2020, **7**, 27-36.